A framework for untangling transient groundwater mixing and travel times

Andrea L. Popp[1,2,3,4], Álvaro Pardo-Álvarez[3], Oliver S. Schilling[3,5], Andreas Scheidegger[1], Stéphanie Musy[7], Morgan Peel[3], Philip Brunner[3], Roland Purtschert[7], Daniel Hunkeler[3], Rolf Kipfer[1,2,8]

[1]Department of Water Resources and Drinking Water, Eawag, Swiss Federal Institute of Aquatic Science and Technology, Überlandstrasse 133, 8600 Dübendorf, Switzerland

[2]Department of Environmental Systems Science, ETH Zurich, 8000 Zurich, Switzerland

[3]Centre d'Hydrogéologie et de Géothermie, University of Neuchâtel, 2000 Neuchâtel, Switzerland

[4]Now at Department of Geosciences, University of Oslo, 0371 Oslo, Norway

[5]Département de géologie et de génie géologique, Université Laval, QC G1V 0A6 Quebec City, Canada

[7]Climate and Environmental Physics, University of Bern, 3012 Bern, Switzerland

[8]Department of Earth Sciences, ETH Zurich, 8000 Zurich, Switzerland

Key Points:

- we introduce a framework to estimate mean travel times of a groundwater fraction consisting of recently infiltrated river water (F_{rw})
- we test the influence of temporally variable end-member tracer concentrations on estimated mixing ratios
- we demonstrate that the streambed has a major control on the travel times of F_{rw}

Corresponding author: Andrea L. Popp, `andrea.popp@geo.uio.no`

–1–

Abstract

Understanding the mixing between surface water and groundwater as well as groundwater travel times in vulnerable aquifers is crucial to sustaining a safe water supply. Age dating tracers used to infer apparent travel times typically refer to the entire groundwater sample. A groundwater sample, however, consists of a mixture of waters with a distribution of travel times. Age dating tracers only reflect the proportion of the water that is under the dating range of the used tracer, thus their interpretation is typically biased. Additionally, end-member mixing models are subject to various sources of uncertainties, which are typically neglected. In this study, we introduce a new framework that untangles groundwater mixing ratios and travel times using a novel combination of in-situ noble gas analyses. We applied this approach during a groundwater pumping test carried out in a pre-alpine Swiss valley. First, we calculated transient mixing ratios between recently infiltrated river water and regional groundwater present in a wellfield, using helium-4 concentrations combined with a Bayesian end-member mixing model. Having identified the groundwater fraction of recently infiltrated river water (F_{rw}) consequently allowed us to infer the travel times from the river to the wellfield, estimated based on radon-222 activities of F_{rw}. Furthermore, we compared the tracer-based estimates of F_{rw} using a calibrated numerical model. We demonstrate (i) that partitioning of major water sources enables a meaningful interpretation of an age dating tracer of the water fraction of interest and (ii) that the streambed has a major control on the estimated travel times.

1 Introduction

Climate change is anticipated to alter the seasonality and quantity of water resources in mountainous regions (e.g., Hock et al., 2019) by affecting snow cover dynamics (e.g., Fiddes et al., 2019), glacier melt (e.g., Huss & Hock, 2015), groundwater storage (Cochand et al., 2019) and river discharge (e.g., Addor et al., 2014; Blöschl et al., 2019; Michel et al., 2020). Although these changes will profoundly influence groundwater recharge and discharge in mountainous environments (Hayashi, 2019), they have largely been ignored so far (Somers et al., 2019). Since surface water and groundwater resources are closely coupled, an improved understanding of surface water-groundwater interactions is highly relevant for a sustainable water governance as well as for water-dependent ecosystems in mountainous regions (e.g., Holman, 2006; Krause et al., 2014; Schilling et al., 2020).

–2–

Within the last two decades, studies on river-aquifer exchange dynamics have substantially improved the understanding of the drivers (e.g., river discharge) and controls (e.g., riverbed hydraulic conductivity) of water exchange patterns and their impact on biogeochemical cycling of solutes (e.g., reviews by Boano et al., 2014, Brunner et al., 2017 and Lewandowski et al., 2019 and references therein). Particularly, the continued recognition and investigation of riverbed dynamics as key controls on river-aquifer exchange have brought substantial scientific progress in the field of surface water-groundwater interactions (e.g., Mutiti & Levy, 2010; Tang et al., 2018). However, the spatiotemporal dynamics of surface water-groundwater interactions still remain elusive, mainly due to a lack of high-resolution field data (Barthel & Banzhaf, 2016; Boano et al., 2014; Brunner et al., 2017; Krause et al., 2014; Partington et al., 2017). Consequently, further progress for an improved conceptual understanding as well as model development (which depends on high-resolution field data for model calibration and validation) is limited by the quantity and quality of data available (e.g., Barthel & Banzhaf, 2016; Paniconi & Putti, 2015; Schilling, Cook, & Brunner, 2019).

Environmental tracers such as stable water isotopes or dissolved noble gases have been proven to be highly beneficial to study groundwater flow-paths, travel times and water source partitioning. These tracers deliver an integrated signal over the entire catchment and thus carry important information on water flow paths on large scales (Cook & Herczeg, 2000; Jasechko, 2019; Sprenger et al., 2019 and references therein). Therefore, recent review papers (Brunner et al., 2017; Jasechko, 2019; Schilling, Cook, & Brunner, 2019; Sprenger et al., 2019) emphasize the need for novel, more efficient (isotope) tracer measurement techniques to enhance the understanding of complex feedback mechanisms occurring in river-aquifer systems. Fortunately, recent advances in tracer-based hydrological modeling (e.g., Schilling et al., 2017) have proceeded synchronously with rapid methodological developments in tracer hydrology (Brunner et al., 2017; Paniconi & Putti, 2015)—the latter allowing for high-resolution (e.g., multiple measurements per hour), on-site sampling of stable water isotopes (e.g., Von Freyberg et al., 2017; Herbstritt et al., 2019) or dissolved noble gases (e.g., Mächler et al., 2012). One such technique enabling high-resolution (noble) gas analysis is a recently developed Gas Equilibrium-Membrane Inlet Mass Spectrometer (GE-MIMS; Brennwald et al., 2016) system, which can analyze a multitude of reactive and noble gas species including helium-4 (^{4}He). Noble gases analyzed with a portable mass spectrometry have shed light on various hydro-

–3–

logical processes within recent years (e.g., Chatton et al., 2017; Hoffmann et al., 2020; Popp et al., 2020; Schilling et al., 2021; Vautier et al., 2020). Likewise, the noble gas radon-222 (^{222}Rn) is another often used tracer to study surface water-groundwater interactions (e.g., Gleeson et al., 2018). With a half-life of 3.8 days, ^{222}Rn can be used to assess apparent travel times (from here on referred to as travel times or TTs) of up to ~15 days of infiltrating river water to groundwater (e.g., Hoehn & Von Gunten, 1989).

However, an accurate interpretation of age dating tracers such as ^{222}Rn activities is inherently challenging because every water sample consists of a mixture of waters with various ages (e.g., Cook & Herczeg, 2000; Jasechko, 2019; Sprenger et al., 2019). Thus, disentangling major flow paths and identifying groundwater mixing processes is key to allow for an accurate interpretation of travel times using age dating tracers (e.g., Sprenger et al., 2019).

The ongoing evolution of mixing models for source partitioning within the hydrological sciences (e.g., Beria et al., 2020; Popp et al., 2019) and beyond (e.g., Stock et al., 2018) provides an often neglected set of toolboxes to account for the various sources of uncertainties related to mixing models. One major limitation of groundwater mixing modeling is to identify end-members correctly and the inability to observe end-members over time (e.g., Carrera et al., 2004; Delsman et al., 2013; McCallum et al., 2010). The assumption of constant end-members cannot be verified or falsified if tracer time-series are unavailable. In fast changing systems though, end-members might in fact be transient. Moreover, a delay between the time a source enters the system and the time it is observed in the mixture is rarely considered (Beria et al., 2020).

In this study, we present a framework with the key objective to determine travel times of a groundwater fraction consisting of recently infiltrated river water (F_{rw}) by first, assessing groundwater mixing between infiltrated river water and regional groundwater using ^{4}He concentrations combined with a Bayesian end-member mixing model (Popp et al., 2019) and second, inferring transient travel times of F_{rw} employing the mixing adjusted ^{222}Rn activities of F_{rw}. To this end, we continuously analyzed dissolved noble gases (^{4}He, ^{222}Rn) on-site during a pumping test lasting seven weeks conducted at a well-field used for the drinking water supply of Bern, Switzerland. The obtained data set is unique in that it provides high-resolution time series of noble gas concentrations for an end-member and the water mixture. Finally, to test our assumptions as well as to val-

–4–

idate the tracer-based results, we compared groundwater mixing ratios obtained from the noble gas analysis with those derived from a fully-coupled and calibrated numerical surface water-groundwater model of the wellfield built in HydroGeoSphere (HGS; Aquanty Inc., 2015).

2 Materials and Methods

2.1 Site Description

This study was conducted in the alluvial catchment of the river Emme, located at the northern margin of the Swiss Alps (Figure 1). We focus on the lower part of the catchment, which consists of the river Emme and the underlying alluvial aquifer. The river exhibits a coarse gravel and sand riverbed with a very dynamic discharge, which is usually highest during snowmelt from April to May (Käser & Hunkeler, 2015).
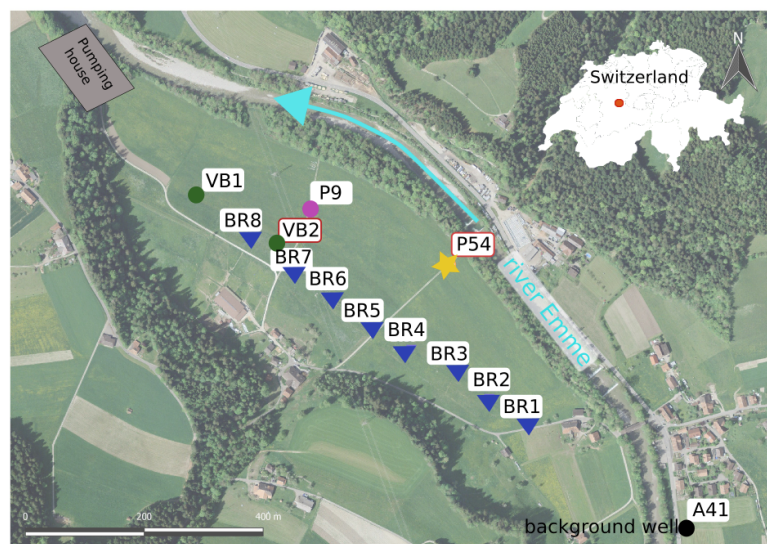

Figure 1. Study area showing the pumping well gallery (BR1–BR8 in blue), two newly installed pumping wells (VB1 and VB2 in green), the location of the pumping house as well as the piezometers P54 (orange), P9 (magenta) and A41 (black). The red dot on the Swiss map indicates the location of the study site.

The alluvial aquifer has an average thickness of about 25 m and can extend up to 46 m. At our study location, the valley is between 200 m and 400 m wide (Würsten, 1991). The upper part of the aquifer is predominantly unconfined, and is filled with coarse sandy

–5–

gravel and cobbles with variable fractions of silt. The saturated hydraulic conductivity of the alluvial aquifer is relatively high ($\sim$500 m/d), compared to the estimated mean hydraulic conductivity of the river bed ($\sim$2.5 m/d) (Schilling et al., 2017). The lower part of the alluvium overlying the bedrock consists of up to 3 m thick silty material, which hydraulically disconnects the bedrock from the alluvial aquifer (Blau & Muchenberger, 1997).

A wellfield consisting of 8 wells (BR1–BR8), aligned in parallel to the river Emme abstracts on average a total of 24 000 L/min of groundwater (Figure 1). Wells BR1 to BR3 pump water from 10 m depth, whereas wells BR4 to BR8 withdraw water from 15 m depth (Käser & Hunkeler, 2015).

Water source partitioning as well as groundwater travel times at this study site are particularly important in the context of current and projected environmental changes. Michel et al. (2020), for example, found that between 1999 and 2018 the annual discharge of the Emme already decreased each decade by 12±4%. Additionally, Addor et al. (2014) showed that river discharge in the Emmental catchment is projected to further decrease by 25–45% in summer (for the years 2070-2099) in response to increasing air temperatures. Changes in river discharge naturally also alter groundwater recharge patterns and are likely to impact water quality (Hock et al., 2019). Consequently, anticipated environmental changes are expected to negatively affect the drinking water production of the study area.

2.2 Controlled Forcing of the System through a Pumping Test

From January 15 to February 26, 2019, a pumping test was conducted, primarily using two newly installed wells (VB1=41 m deep and VB2=26 m deep, screened from 6 m depth to the bottom of the borehole) as well as already existing wells (BR4–BR8; Figure 1).

Figures 2a) and 2b) show the dynamics of the prevailing hydraulic conditions during the pumping test, and d) shows the water temperatures. Figure 2c) depicts the three main phases of the pumping test: (1) January 15 marks the beginning of the pumping test when pumping started with 16 000 L/min equally withdrawn from VB1 and VB2, and was gradually increased to 26 000 L/min (14 000 L/min from VB1 and 12 000 L/min from VB2) until January 18; (2) from February 12 to 26 pumping was further increased
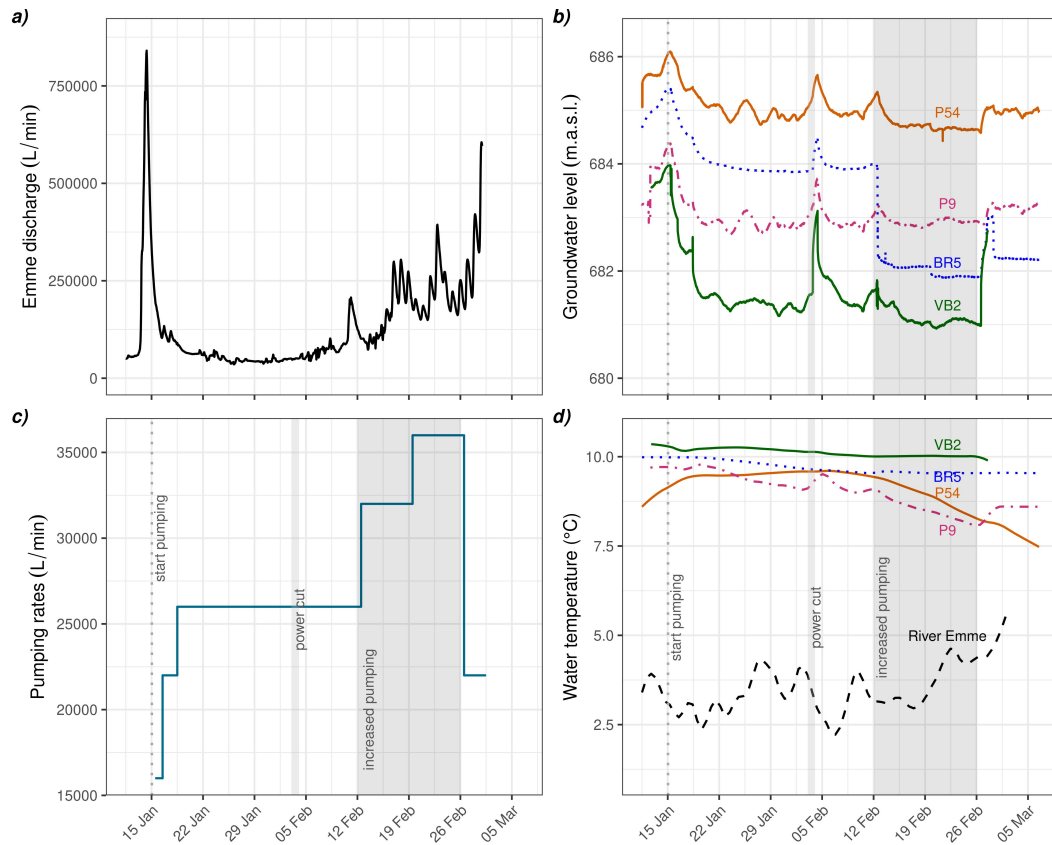
–6–

Figure 2. Prevailing conditions during the experiment: (a) the discharge of the Emme (recorded at Heidbhl-Eggiwil ∼8 km upstream of the study site), (b) groundwater levels of P54 (orange), VB2 (green), BR5 (dotted, blue) and P9 (dashed, magenta), (c) the total sum of groundwater pumped and (d) water temperatures of P54, VB2, BR5, P9 and the river Emme (dashed, black). The dark gray segment indicates the period of increased pumping (February 12–26). Light gray bands indicate an electric power cut occurring at the study site, which caused a shutdown of all wells from February 3, 6:30 p.m., to the following morning at 10 a.m.

to reach an overall maximum pumping rate of 36 000 L/min by employing BR4 to BR8 (11 000 L/min) in addition to VB1 (14 000 L/min) and VB2 (11 000 L/min); (3) on February 26 the pumping test was completed and the pumping regime at the drinking water production site went back to normal operating conditions (i.e., using BR1–BR8 only). Please note that there was a complete shutdown of all pumps from January 10 to 15. All pumping rate data can be found in Table S1 (Supporting Information).

2.3 Methodological Framework

Figure 3 illustrates the framework introduced by this study. The aim is to first partition the major groundwater sources (red box) to ultimately infer the travel times of the recently infiltrated water fraction (F_{rw}; blue box). The following sections explain the used tracer data and modeling approaches.
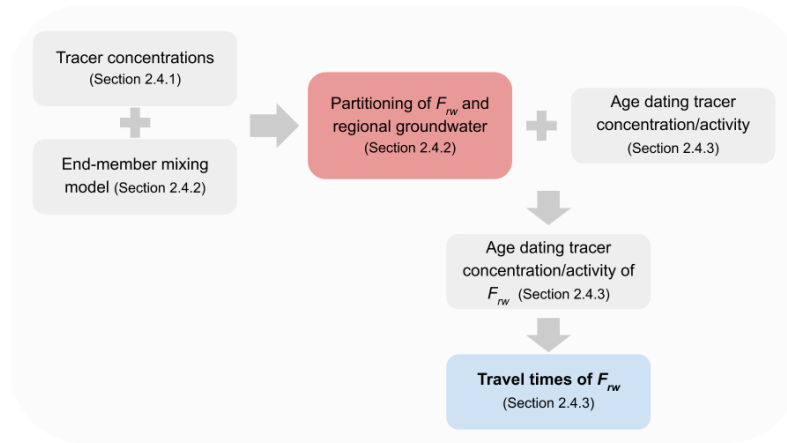

Figure 3. Framework illustrating the approach of determining travel times of a water fraction based on the previous estimation of mixing ratios using a combination of tracer data and end-member mixing modeling.

2.4 Tracer-Based Approach

2.4.1 Theory and Dissolved (Noble) Gas Analyses

The activities of the radioactive noble gas ^{222}Rn increase non-linearly in groundwater and eventually reach a secular equilibrium after $\sim$20 days ($\sim$5 half-lives; Krishnaswami et al., 1982). The Earth's atmosphere has virtually no source of ^{222}Rn, therefore, water in equilibrium with the atmosphere is practically devoid of radon (e.g., Cook & Herczeg, 2000; Figure 4). The absence of ^{222}Rn in air-equilibrated water and its short half-life render ^{222}Rn an excellent tracer to study surface water-groundwater interactions (e.g., Bourke et al., 2014; Gleeson et al., 2018; Hoehn et al., 1992).
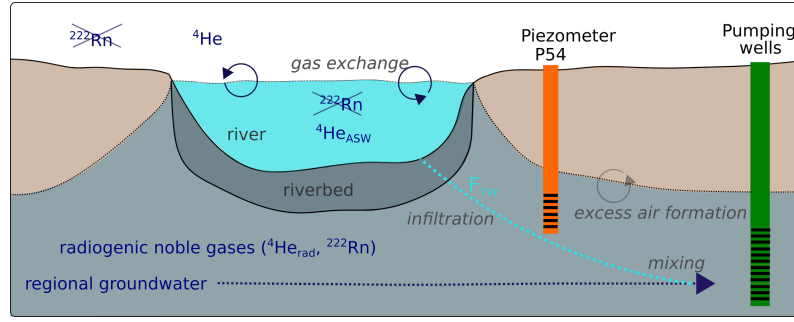
–8–

Figure 4. Conceptual model of processes (in italic) affecting the noble gas composition of groundwater at a losing stream reach: the ^{4}He concentration of the river is solely affected by gas exchange with the atmosphere; once the river infiltrates, ^{4}He is added due to excess air formation. The admixture of ^{4}He$_{rad}$-enriched older groundwater causes a further increase in ^{4}He concentrations. ^{222}Rn starts to accumulate once river water infiltrates. Please note that the groundwater flow paths are mostly parallel to the river (see Figure S4, SI).

Different to ^{222}Rn, ^{4}He is a stable noble gas (isotope), which is either of atmospheric or radiogenic origin (Figure 4). The concentration of ^{4}He dissolved in groundwater (^{4}He$_{gw}$) is given by

$$^4\text{He}_{gw} = {}^4\text{He}_{asw} + {}^4\text{He}_{ea} + {}^4\text{He}_{rad} \tag{1}$$

where ^{4}He$_{asw}$ corresponds to the helium in air-saturated water (ASW) at a given water temperature, pressure and salinity, ^{4}He$_{ea}$ is helium originating from excess air formation (i.e., the partial dissolution of air entrapment at recharge and water table fluctuations; Heaton & Vogel, 1981) and ^{4}He$_{rad}$ represents radiogenic helium accumulated underground (e.g., Cook & Herczeg, 2000).

Recently infiltrated river water presumably does not contain any ^{4}He$_{rad}$ (Gardner et al., 2011). Thus, any excess in ^{4}He$_{gw}$ (relative to atmospheric-derived ^{4}He, i.e., ^{4}He$_{asw}$ and ^{4}He$_{ea}$) indicates an admixture of older groundwater containing ^{4}He$_{rad}$ due to longer travel times (Figure 4). In this study, we assume (i) that the observed dynamics of helium concentrations is governed by changes in excess air formation in end-member 1 (i.e., recently recharged water from the river), (ii) that the helium in end-member 2 (i.e., the regional groundwater) remains constant within the studied wellfield and (iii) that no additional excess air is formed after the point in time when the end-members were analyzed

in the piezometers P54 and A41, respectively. We consequently use the total helium concentration differences between the two end-members for the end-member mixing model, as it is done with any other conservative tracer.

The dissolved (noble) gases were analyzed at two locations: in Piezometer P54 and in the pumping house (Figure 1). P54 serves as a proxy for infiltrated river water due to its close proximity to the Emme ($\sim$50 m). There, a submersible pump (Comet ECO-PLUS_20000) abstracted $\sim$3 L/min from a depth of 6 m (well depth is 8 m with 2 m screen at the bottom). In the pumping house, we first only analyzed water originating from the newly installed pumping well VB2. VB2 is located in about 220 m distance to the river. Water from VB2 was abstracted by two submersible pumps (8 m and 10 m below ground) and parts of it were diverted to the pumping house. The remaining part of the water abstracted at VB2 and all water pumped at VB1 were discharged to the river, thus, the water pumped from VB1 (by two submersible pumps, 8 m and 10 m below ground) was at no point of this experiment contributing to the water mixture analyzed in the pumping house. To increase the pumping rate, the existing Wells BR4-8 were turned on progressively on February 12 (Table S1) and all the pumped water mixture went to the pumping house. At the same time, all water from VB2 was discharged into the river. This means that from February 12 on, the water being analyzed in the pumping house was a water mixture originating from the wellfield (i.e., BR4-8; Table S1). At both locations (i.e., inside the pumping house and inside a wooden hut at P54; Figure S1), we continuously analyzed dissolved ^{222}Rn using a Rad7 instrument (DURRIDGE, 2019) as well as ^{4}He employing the GE-MIMS system. The two instruments were operated in parallel by allocating $\sim$1.5 L/min of pumped water to each instrument. Sampling resolution of the Rad7 was 30 min per sample and $\sim$10 min per sample for the GE-MIMS. For air-water equilibration, we used commercially available membrane modules (3M Liqui-Cel, 2017) for all instruments. Gas sampling and analysis were conducted in exactly the same way at both locations. More details on continuous noble gas analyses are available in Text S1.

2.4.2 Tracer-Based Mixing Ratios

As previously shown (e.g., Carrera et al., 2004; Delsman et al., 2013; Hooper, 2003; Popp et al., 2019), estimated water mixing ratios based on tracer-aided end-member mixing models can exhibit large uncertainties. Uncertainties can originate, for instance, from

–10–

231 using tracers that are not truly conservative (e.g., Valder et al., 2012), by not identify-

232 ing all end-members correctly (Carrera et al., 2004; Delsman et al., 2013) and because

233 end-members (and their associated tracer signals) are not constant in time (e.g., Hooper

234 et al., 1990). These uncertainties are still often neglected, preventing a meaningful anal-

235 ysis of model errors, which can in turn lead to an erroneous interpretation of the results.

236 To quantify and account for these uncertainties, we applied a Bayesian groundwa-

237 ter mixing approach (see Popp et al., 2019) using hourly aggregated ^{4}He concentrations

238 as tracers. This approach allows to explicitly account for sampling and measurement un-

239 certainties (Popp et al., 2019). The model in this study was simplified by excluding the

240 possibility of unknown end-members based on a sound conceptual understanding of the

241 area from previous studies (Käser & Hunkeler, 2015; Schilling et al., 2017; Tang et al.,

242 2018). Accordingly, we defined two end-members. For the end-member mixing model-

243 ing approach, end-member 1 (E_1) is represented by P54, given its proximity to the river.

244 We thereby assume that E_1 consists entirely of recently infiltrated river water, contain-

245 ing excess air but no ^{4}He$_{rad}$—an assumption that was supported by the numerical model

246 (see Section 3.2). End-member 2 (E_2) is represented by piezometer A41 ($\sim$20m deep;

247 Figure 1), that previously served as background piezometer for regional groundwater by

248 Schilling et al. (2017). There are no high-resolution tracer data available for the back-

249 ground well. However, following Schilling et al. (2017), time-series data seem dispens-

250 able since this piezometer was identified to hardly be affected by seasonal changes or ground-

251 water pumping. The ^{4}He concentration of end-member E_2 is thus assumed to be con-

252 stant over time, which is why there is no time dependency given for E_2 in Equation 2.

253 The measured ^{4}He concentrations at E_1, however, are dynamic (Figure 5). Consequently,

254 we assume, similar to Brewer et al. (2002), that for every point in time t the following

255 relationship holds for the water mixture $C_{mix(t)}$ observed in the pumping house:

$$C_{mix(t)} = F_{rw(t)}\, \tilde{C}_{E_1(t)} + F_{ogw(t)}\, C_{E_2} \tag{2}$$

256 where F_{rw} is the fraction of recently infiltrated river water, F_{ogw} the fraction of

257 older, regional groundwater, C_{E_2} is the concentration of a tracer observed at end-member

258 E_2 and $\tilde{C}_{E_1(t)}$ is a <u>time averaged</u> concentration observed at the dynamic end-member

259 E_1. Equation 2 is solved for F_{rw}, while F_{ogw} is per definition 1-F_{rw}.

²⁶⁰ Since the transit time between end-member 1 and the wellfield is unknown, we tested

²⁶¹ the sensitivity of estimated mixing ratios to potential delays, that is, the time the wa-

²⁶² ter/tracer needs to travel from P54 to the wellfield. To this end, we imposed different

²⁶³ time lags (1–10 days) with one day increments on the tracer used for the mixing model,

²⁶⁴ where the tracer time series was shifted for a particular time lag and the mixing ratios

²⁶⁵ were calculated for the according tracer concentrations shifted in time. The ten days rep-

²⁶⁶ resent the upper end of the possible time lag—an assumption based on artificial tracer

²⁶⁷ tests (using uranine and naphthionat), which were conducted as part of the pumping ex-

²⁶⁸ periment. The artificial tracer tests suggest groundwater flow rates between 45 and 100 m/d

²⁶⁹ within the study domain. To represent the delay in flow time and dispersion, the mix-

²⁷⁰ ing ratios are calculated with the averaged concentration

$$\tilde{C}_{E_1(t)} = \int_0^\infty w(\tau)\, C_{E_1(t-\tau)}\, \mathrm{d}\tau \tag{3}$$

²⁷¹ where $w(\tau)$ is the density function of a gamma distribution with a mean μ_{delay} and

²⁷² a relative standard deviation $\sigma_{r,\mathrm{delay}}$, where σ is defined as 15% of μ. We choose a gamma

²⁷³ distribution, however, a different parametric family, for instance an inverse Gaussian dis-

²⁷⁴ tribution, would lead to the same results as long as the mode is far from zero (which is

²⁷⁵ the case for how we defined the distribution). Therefore, the choice of the parametric

²⁷⁶ family is negligible if the shape parameter is larger than one. As prior we used a uni-

²⁷⁷ form Dirichlet distribution with alpha=1.

²⁷⁸ The only constraints of our mixing modeling approach are that the mixing ratios

²⁷⁹ are positive and sum up to one. Mixing ratios are estimated for every point in time in-

²⁸⁰ dependently. Deviations from equation 2 are assumed to stem only from observational

²⁸¹ errors due to tracer-related uncertainties. These errors were modeled as normal distri-

²⁸² butions with relative standard deviations.

²⁸³ Employing the Bayesian mixing model, we assumed an overall uncertainty of 5%

²⁸⁴ for E_1 and for each individual measurement of the analyzed water mixtures. These un-

²⁸⁵ certainties are based on analytical errors ($\sim$2%) plus $\sim$3% due to inconsistencies in sam-

²⁸⁶ pling and analytical procedures. For E_2, we allocated an overall uncertainty of 10% due

²⁸⁷ to the strong assumptions of having steady-state conditions at this location and that A41

²⁸⁸ truly represents regional groundwater (similar to Popp et al., 2019). The aforementioned

²⁸⁹ uncertainties also acknowledge the possibility of other water sources (such as snowmelt)

290 contributing to the water mixture, which we assume to have a negligible impact on the

291 tracer concentrations.

292 This approach consequently allowed us to estimate the recently infiltrated river wa-

293 ter fraction of the groundwater mixtures analyzed in the pumping house.

2.4.3 Estimating Travel Times of F_{rw}

295 Having estimated F_{rw}, we were able to determine the radon activities originating

296 from this water fraction ($Rn_{(F_{rw})}$) assuming that ^{222}Rn activities of E_2 (Rn_{E2}) equal those

297 of the background well. We assume that the water in the background well exhibits steady-

298 state ^{222}Rn activities due to its long residence time (Schilling et al., 2017):

$$Rn_{(F_{rw(t)})} = \frac{(Rn_{mix(t)} - (1 - F_{rw(t)}) * Rn_{(E_2)})}{F_{rw(t)}} \quad (4)$$

299 where $Rn_{(mix)}$ is the ^{222}Rn activity of the water mixture analyzed in the pumping house.

300 Consequently, we estimated travel times in days (d) using hourly aggregated ^{222}Rn

301 activities (number of observations, $n=911$) analyzed in the pumping house by means of

302 the ^{222}Rn in-growth approach (Hoehn & Von Gunten, 1989; see Figure S2 for the in-growth

303 curve):

$$TT_{(t)} = \lambda^{-1} * ln \frac{(Rn_{(E_2)} - Rn_{(river)})}{(Rn_{(E_2)} - Rn_{(F_{rw(t)})})} \quad (5)$$

304 where λ is the radioactive decay constant (0.183 day^{-1}; Hoehn & Von Gunten, 1989)

305 and $Rn_{(river)}$ corresponds to the mean radon activity analyzed in the river Emme. Please

306 note that the ^{222}Rn activities of P54 are not included in the calculation of the travel times.

307 While the water of P54 represents an end-member for the ^4He concentrations, it is not

308 an end-member for ^{222}Rn due to its short half-life.

2.5 Simulation-Based Approach

310 To compare and validate tracer-based mixing ratios with those from a calibrated

311 numerical model (from here on referred to as simulation-based mixing ratios), we used

312 a model built in HGS combined with the Hydraulic Mixing-Cell flow tracking tool (HMC;

313 Partington et al., 2011) to determine water mixing throughout the model domain.

–13–

HGS is able to simulate both surface water and groundwater flow in a fully-integrated way, that means, precipitation partitions into all parts of the water cycle (e.g., groundwater recharge, snow, streamflow, evapotranspiration) in a physically-based manner, making it unnecessary to artificially impose these components as boundary conditions. HGS solves a modified version of the Richard's equation using the van Genuchten parametrization. This allows for the simulation of variably saturated subsurface flow, which is particularly important when simulating river-aquifer interactions (Brunner & Simmons, 2012; Schilling et al., 2017). Different to particle tracking, HMC is based on an the efficient mixing cell approach (Harrington et al., 1999; Rao & Hathaway, 1989), automatically tracking all water that enters the model domain via specified boundary conditions. HMC thus provides transient mixing ratios of all water sources in every model cell at every time step, and this for marginal extra computational costs (Partington et al., 2011).

We adopted the existing model built and calibrated by Schilling et al. (2017), thus our model setup equals the description therein. Before the transient simulation of the pumping experiment, a quasi-steady-state simulation with constant forcing for 2 586 days (corresponding to the forcing observed at the beginning of the transient simulation period) was carried out, to obtain an equilibrated initial distribution of water sources for subsequent transient HMC analyses. For the transient simulations, all boundary conditions (i.e., river discharge, groundwater heads, precipitation, air temperature and snow) were updated according to corresponding values at the time of our experiment. In contrast to Schilling et al. (2017), we explicitly simulated snow accumulation and snowmelt (Jonas et al., 2009; Magnusson et al., 2014; Schilling, Park, et al., 2019), because winter conditions were prevalent during a significant part of our experiment.

3 Results

3.1 Continuously Analyzed Dissolved (Noble) Gases

Figure 5 shows the ^{222}Rn activities (a) and ^{4}He concentrations (b) synoptically analyzed at P54 and in the pumping house. The illustrated data were hourly aggregated (single data points) and smoothed to facilitate visualization (data line). For data smoothing, we applied local polynomial regression fitting (i.e., LOESS; Jacoby, 2000) to all data sets shown in Figures 5 and 7 to reduce noise and increase readability.

As expected, ^{222}Rn activities and ^{4}He concentrations are lower at P54 than the observations made in the pumping house, except for a short period in February. The ^{222}Rn activities observed in the pumping house temporarily reached the secular equilibrium (i.e., $12\,500\pm1\,300$ Bq/m^3 observed at A41, $n=14$). ^{222}Rn activities recorded at P54, however, have not reached the secular equilibrium. The activities obtained at P54 indicate the relative long time the river water needs to pass through the streambed, which has a low hydraulic conductivity compared to the aquifer (Schilling et al., 2017; Tang et al., 2018). ^{4}He concentrations observed at P54 are closer aligned to the ^{4}He concentrations of air-saturated water (ASW) at 3°C (reflecting the ^{4}He concentration of the prevalent mean Emme water temperature) than the background well.

Although both tracers (^{4}He and ^{222}Rn) exhibit temporal fluctuations, the overall trend shows a decrease in both tracers for the duration of our experiment. Please note that we assumed the tracer activity/concentration for end-member 2 (i.e., the background well) to be constant over time. Also note that we did not detect any considerable ^{222}Rn activities in the river Emme during sporadic sampling (mean activity 199 ± 139 Bq/m^3, $n=13$), which indicates that the river was not gaining any relevant amounts of groundwater during the period of our experiment.

3.2 Tracer-Based and Simulation-Based Estimates of F_{rw}

Figure 6 shows the estimated fraction of recently infiltrated river water for the well-field (i.e., water mixture analyzed in the pumping house) inferred from the tracer-based (various colours) and the simulation-based approach (dashed, black). Since F_{rw} observed in the pumping house results from a mixture of waters coming from different pumping wells, we calculated the simulated F_{rw} values (derived from the numerical model) as a weighted mean according to the relative water contribution from each well to the water mixture. The dashed black line in Figure 6 thus illustrates a weighted mean of F_{rw} equivalent to the groundwater mixture analyzed in the pumping house.

Figure 5 highlights that the assumption of time-invariant end-members does not hold for our data because the tracer concentrations observed at P54 vary within the observation period. However, Figure 6 shows no distinct differences in mixing ratios when imposing different time delays (i.e., 1-10 days), suggesting that the influence of a potential time lag on the estimated mixing ratios is negligible. Consequently, all data regard-
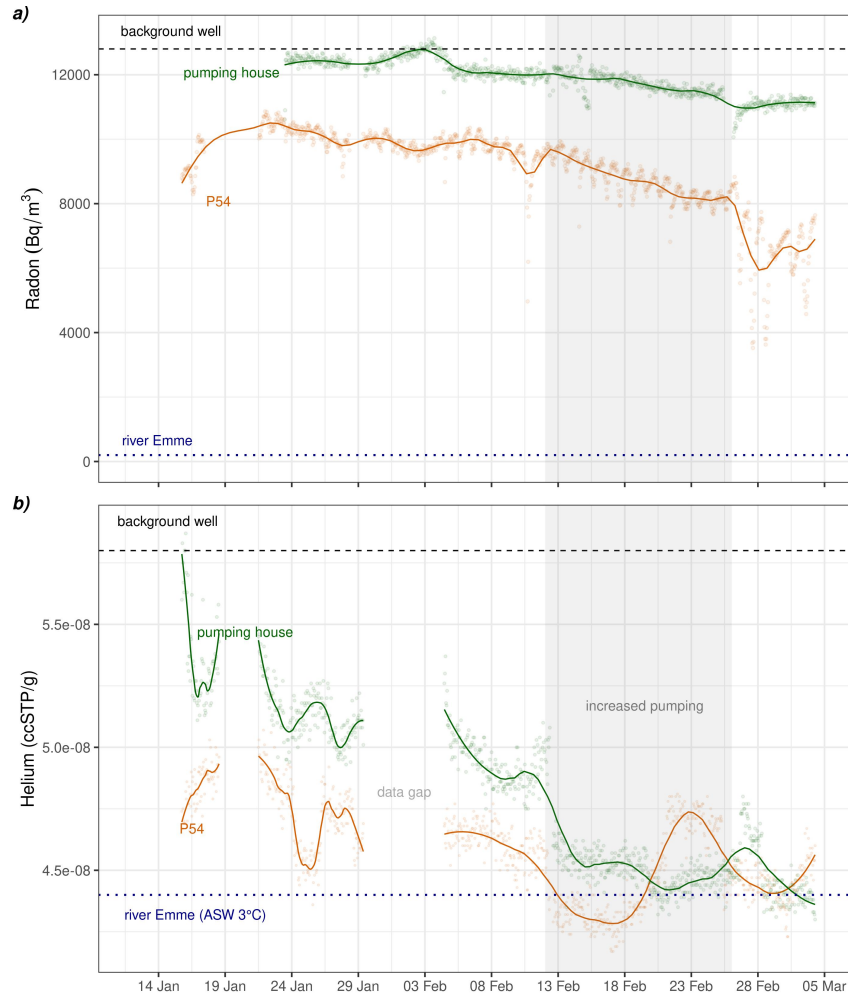
–15–

Figure 5. (a) ^{222}Rn activities and (b) ^{4}He concentrations continuously analyzed at P54 (orange) and in the pumping house (green); the background well (A41, black dashed line) represents regional groundwater; ASW (blue dotted line) represents the average ^{4}He concentration of the river water. Gray segments indicate the period of increased pumping. Note that no error bars are shown because the analytical uncertainty of both tracer methods is lower than the temporal variability seen in the data points.

Table 1. Estimates of F_{rw} as well as travel times during the three major phases of the pumping test. Uncertainty of the simulated F_{rw} refers to the standard deviation of the simulated mean over the respective period.

	Increased pumping		
	before	during	after
Tracer-based F_{rw} (%)	57±25	75±21	76±20
Simulated F_{rw} (%)	74±7	67±3	73±3
TT (d)	14±4	12±3	9±2

³⁷⁵ ing F_{rw} correspond from here on to the estimated mixing ratios with no imposed time
³⁷⁶ lag (pink data shown in Figure 6).

³⁷⁷   Generally, the tracer-based and simulation-based mixing ratios agree reasonably
³⁷⁸ well within the calculated uncertainties, except for the beginning of the experiment. For
³⁷⁹ the entire duration of the experiment, the tracer-based and simulation-based estimates
³⁸⁰ predict an average of 67±23% and 70±4% of water originating from recently infiltrated
³⁸¹ river water, respectively. The experiment can be divided in three major phases: before,
³⁸² during and after the pumping was increased (Table 1 and Figure 2c). The tracer-based
³⁸³ calculations show an increase from about 57±25% (period before the pumping increased)
³⁸⁴ to a mean value of 75±21% for the time of increased pumping. After the pumping regime
³⁸⁵ went back to normal operation conditions, F_{rw} first slightly dropped but then increased
³⁸⁶ again. The simulated estimates of F_{rw} show a different trend: after pumping increased,
³⁸⁷ estimates slightly decreased from 74±7% to 67±3%. In the last phase, simulated esti-
³⁸⁸ mates of F_{rw} slightly increased again to 73±3%. Although these differences fall in the
³⁸⁹ range of the estimated uncertainties, the trends of the tracer-based and simulation-based
³⁹⁰ mixing ratios do not necessarily correlate (see Discussion for model limitations).

³⁹¹   Mixing ratios simulated at P54 confirm that its water consists almost exclusively
³⁹² (~90%) of infiltrated river water. Thus, the assumption to use ⁴He concentrations of P54
³⁹³ to characterize the ⁴He concentrations of F_{rw} for the groundwater mixing model seems
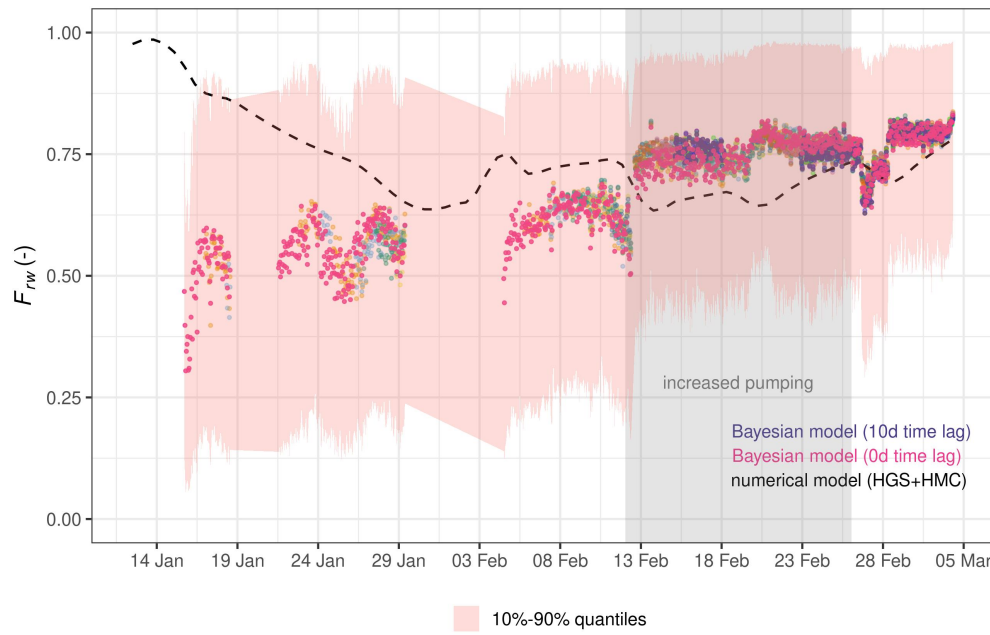³⁹⁴ justified.

Figure 6. Estimates of F_{rw} (for the water mixture analyzed in the pumping house) from the numerical model (dashed, black line) and from the tracer-based Bayesian model with no time lag (pink), a 10 days time lag (dark-blue) and 1 to 9 days time lag scenarios (various colors). Error bars indicate the 10% and 90% quantiles derived from the Bayesian model (no time lag).

3.3 Travel Times of F_{rw}

Knowing the fraction of river water within the pumped groundwater, we can use the ^{222}Rn activities of F_{rw} to infer the travel times of F_{rw} to the wellfield. In accordance with the decreasing ^{222}Rn activities observed at P54 and the pumping house (Figures 5 and 7), the estimated TTs show the same decreasing trend over time. On average, the travel time from the river to the wellfield is in the range of 12±3 days. With 14±4 days, the period before the pumping was increased showed the highest mean travel time (Table 1). After pumping was increased, TTs generally decrease until the end of the experiment. Towards the end of February, we obtained travel times as low as 7±2 days.

From the ^{222}Rn activities shown in Figure 5a) it becomes apparent that the recently recharged river water (observed in P54) has already accumulated a substantial amount of the total ^{222}Rn measured in the pumping house, which indicates that a large portion of the total travel time occurs between the stream and P54. Consequently, the travel time between P54 and the wellfield is comparatively fast. This phenomena can be explained by the lower hydraulic conductivity of the riverbed that the infiltrating river water needs to pass first. For the remaining distance between P54 and the wellfield ($\sim$200-300m), the recently recharged river water only takes a few days, which aligns well with the results of the artificial tracer test suggesting groundwater flow rates of up to 100 m/d within the aquifer.

Finally, the average travel time (12±3 days; Table 1) using the mixing-corrected ^{222}Rn activities aligns well with the travel time obtained through the artificial tracer test, which revealed a travel time from the injection well (i.e., A41) to VB2 of $\sim$7 days (Figure S3). Since the tracer was directly injected into the groundwater, the travel time between the point of injection and VB2 is expected to be lower than the TT of F_{rw} because the river water has to pass the low hydraulic conductivity zone of the riverbed before entering the aquifer.

4 Discussion

4.1 Validation of Tracer-Based and Simulation-Based Mixing Ratios

The estimated mixing ratios of the tracer-based and simulation-based approaches agree acceptably well, considering the underlying assumptions and associated uncertainties of both approaches (Figure 6). At the beginning of the pumping test, however, the
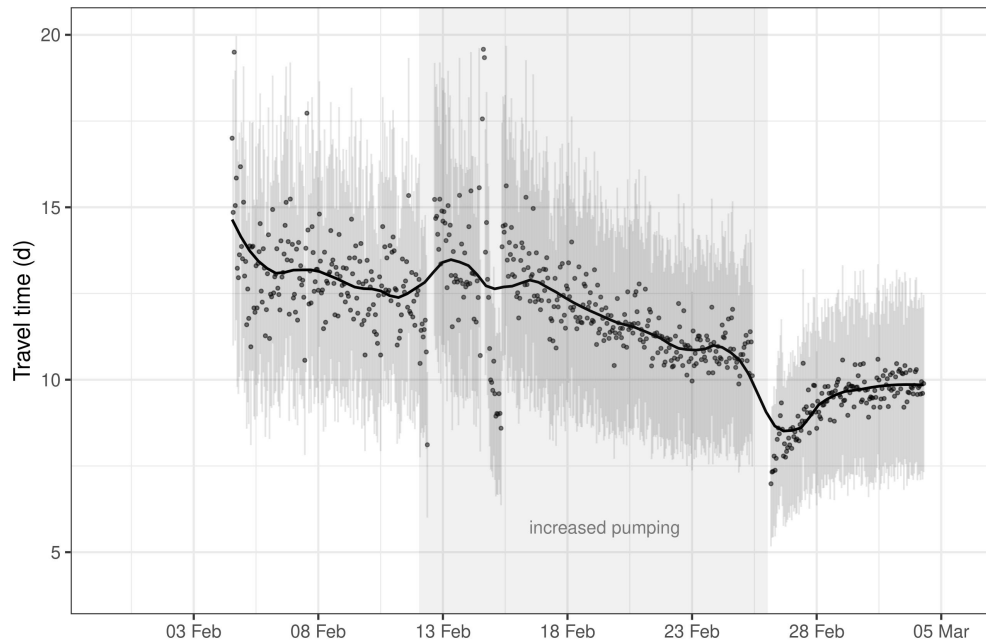
–19–

Figure 7. Estimated TTs of F_{rw} for the water mixture analyzed in the pumping house. Error bars indicate propagated uncertainty derived from the Bayesian mixing model (no time lag) and analytical uncertainties.

simulated and tracer-based mixing ratios show considerable dissimilarities. There are also contrasting effects between the two approaches during the three different phases of the pumping test (Table 1): the simulations generally show lower estimates of F_{rw} during the increased pumping period, whereas the tracer-based estimates of F_{rw} increase steadily from the first to the third phase. These differences most likely reflect the heterogeneity (e.g., causing preferential flow paths) of the aquifer, which the numerical model does not adequately reproduce because the aquifer and the streambed are both represented by homogeneous hydraulic conductivities.

Besides comparing tracer-based and simulation-based mixing ratios, we can also compare our tracer-based results with results of Schilling et al. (2017). Using a combination of different tracers including ^{222}Rn, ^{37}argon, ^{3}He/^{4}He and noble gas recharge temperatures, Schilling et al. (2017) observed fractions of recently infiltrated river water within a similar range (between 70–80%) at BR7. Consequently, our estimates of F_{rw} are agree reasonably well with previous results.

440   The cause for the rise in ^{4}He concentrations observed in P54 from February 19 to

441 February 23 remains unclear and is not possible to explain without another conserva-

442 tive tracer available. The lack of such is a major shortcoming of this study. We intended

443 to use electrical conductivity as additional conservative tracer, however, the probe we

444 installed in piezometer P54 was not working properly and thus yielded no usable data.

445 Also, the water temperature measurements (Figure 2d) do not provide any additional

446 insight on this matter.

4.2 Impact of Controlled Forcing on Groundwater Levels, Mixing Ratios and Travel Times

449   Figures 2b) and 2c) show that groundwater pumping clearly has an effect on ground-

450 water levels and a minor effect on water temperatures. During the increased pumping

451 phase the tracer-based estimates show an increase in F_{rw} of about 18%, while the es-

452 timated travel times decrease about 14% in comparison to the previous phase (Table 1s).

453 These changes are most likely related to the change in the pumping regime once pump-

454 ing was increased because the analyzed water originated no longer from VB2 but from

455 a mixture of waters from different wells that are about 10 m less deep than VB2. We

456 hypothesize that the elevated well depths, in turn, most likely influence F_{rw}.

457   From previous (e.g., Schilling et al., 2017; Tang et al., 2018) and our own results,

458 we conclude that groundwater flow paths and travel times exhibit a temporal variabil-

459 ity, which are only to some extend governed by the applied groundwater pumping rates.

460 We explain this relatively low sensitivity against hydraulic forcing by the high hydraulic

461 conductivity of an aquifer with a large transmissivity and thus high storage capacity: the

462 high hydraulic conductivity enables large amounts of river water to infiltrate at various

463 locations upstream of the catchment. An infiltration spread over a large area results in

464 an overall large F_{rw} in the groundwater mixture, regardless of the intensity of the ap-

465 plied groundwater pumping. Another factor is the high hydraulic gradient (Figures 2b),

466 which induces a high groundwater flux relative to pumping. Moreover, temporal trends

467 of F_{rw} (e.g., increase in F_{rw} and decrease in travel times) also seem partially controlled

468 by the rise in river discharge (thereby enhancing infiltration rates) over the duration of

469 this experiment (Figure 2a). This assumption is also supported by the increase in mix-

470 ing ratios (Figure 6) within the last days of the experiment (after pumping was shut-down),

471 which can only be explained by an increased river discharge (Figure 2a) and not by any

–21–

472 pumping-related activities. Consequently, river discharge appears to have a large con-

473 trol of mixing between river water and groundwater in the studied aquifer. We would

474 like to highlight though that the mixing ratios and travel times are governed by several

475 processes (i.e., the changes in pumping rates and pumping wells and their depths as well

476 as the river discharge). The methods we used here do not allow us to disentangle the dif-

477 ferent effects, which is, however, also beyond the purpose of this study.

4.3 Limitations of Estimated F_{rw} and Travel Times

479 Despite the acceptable agreement of estimated mixing ratios by two independently-

480 executed methods, this study has several limitations. Since any water sample is a mix-

481 ture of waters with a distribution of travel times, any interpretation of tracer data is chal-

482 lenging and potentially erroneous (e.g., Jasechko, 2019; Sprenger et al., 2019). Ideally,

483 we would have analyzed multiple age-dating tracers (e.g., ^{37}argon, ^{35}sulfur and ^{3}H/^{3}He)

484 to capture a wider range of potential water ages. However, such tracer studies cannot

485 be carried out at a high spatial and temporal resolution since they are typically costly

486 and unfeasible to sample with a high temporal resolution. Also, only specialized labo-

487 ratories are able to conduct such analyses. Additionally, it would have been very help-

488 ful to better constrain the mixing ratios by using a combination of conservative tracers

489 because the tracer set size and composition can influence the estimated mixing ratios (Barthold

490 et al., 2011; Popp et al., 2019).

491 We are also aware that not everyone has two portable GE-MIMS systems and two

492 Rad7 instruments available. Another potential way of using the introduced framework

493 would be a combination of high-resolution sampling of other, cheaper conservative trac-

494 ers (e.g., electrical conductivity) and grab sampling of specialized tracers (e.g., noble gases

495 such as ^{4}He or ^{37}argon).

496 Moreover, we acknowledge that the possible dating range of ^{222}Rn might not cap-

497 ture the actual distribution of travel times of F_{rw}. As indicated by the results of this study

498 (Figure 7) and Schilling et al. (2017), travel times temporarily exceed the reliable dat-

499 ing range of ^{222}Rn (i.e., 0-15 days). However, we argue that in the context of drinking

500 water production from bank filtrate, the identification of water fractions younger than

501 two weeks is most relevant. This is particularly true for Switzerland where, according

502 to the water protection law (GSchV, SR 814.201), groundwater used for drinking wa-

–22–

ter production must have a travel time of at least 10 days within the relevant protection zone. Thus, in terms of drinking water supply, a conservative estimate of the lower limit of travel times of recently infiltrated surface water is of the highest interest.

Lastly, we would like to acknowledge the assumption that the infiltration signal at P54 is representative of the entire reach, although the infiltrated river water observed at P54 only integrates a small fraction of the aquifer. By using the tracer signal of P54 we assume that no natural variability of the river bed and bank exists (e.g., variable riverbed thickness or hydraulic conductivity), which could potentially influence stream water infiltration pattern.

5 Conclusions and Implications

The primary goal of this study was to develop a framework (Figure 3) that enables a meaningful interpretation of a water age dating tracer by first partitioning major water sources and second interpreting the age dating tracer concentration/activity of the water fraction of interest. We applied this approach using a combination of in-situ analyzed tracer data and modeling under partially controlled forcing conditions (i.e., a groundwater pumping test). In summary, the study provides the following methodological advancements for tracer hydrology:

- Partitioning major water sources enables the interpretation of an age dating tracer (here ^{222}Rn activities) of the recently infiltrated water fraction (Figure 7).
- We explicitly account for all uncertainties related to model assumptions and tracer measurements by employing a Bayesian mixing model. This approach enables us to quantify model uncertainties, propagate these uncertainties to the estimated travel times and generally allows us to test assumptions posteriori (Figure 6).
- We demonstrate the continuous, on-site use of state-of-the-art tracer techniques to elucidate the transience of water sources and mixtures (Figure 5). Without high-resolution time-series data, the system response to forcing (either in the form of groundwater pumping or increased river discharge) cannot be assessed properly.
- Furthermore, the continuous observation of an end-member demonstrates that the common assumption of constant end-members can be inaccurate. At the same time, testing the sensitivity of the estimated mixing rations to different imposed time lags (i.e., the delay between the time a source/end-member enters the system and

the time it is observed in the mixture) showed that a time lag seems to have negligible influence on the estimated mixing ratios, at least for the studied wellfield and the available dataset.

- Although applied here with two specific tracers, the framework can be used with other suitable tracers (dependent on the system of interest).

Additionally, our results imply the following insights for an improved system understanding of an alluvial, pre-alpine aquifer and water resources management:

- On average, a substantial fraction ($\sim$70%) of abstracted groundwater originates from recently infiltrated river water (Table 1 and Figure 6).
- F_{rw} exhibits travel times in the order of two weeks but can be as low as 7$\pm$2 days (Figure 7).
- Our findings (i.e., observed ^{222}Rn activities) indicate that the streambed has a major control on the travel times of infiltrating stream water (Figure 5a) causing relatively long travel times between the stream and the streambank, relative to the total estimated travel times from the stream to the wellfield.
- All three previous points are highly relevant for drinking water supply systems at similar sites using bank filtrate.

Overall, these findings (particularly the high fraction of F_{rw} in the abstracted groundwater and its short travel times) suggest that the system studied is vulnerable to current and anticipated environmental changes such as increasing contamination and summer droughts.

References

⁵⁷¹ 3M Liqui-Cel. (2017). A high level of consistency and control. Wuppertal, Ger-
many. Retrieved from `http://multimedia.3m.com/mws/media/1412485O/3m`
`-liqui-cel-membrane-contactors-liquid-degasgaslc-1096-pdf`

⁵⁷⁴ Addor, N., Rössler, O., Köplin, N., Huss, M., Weingartner, R., & Seibert, J. (2014).
Robust changes and sources of uncertainty in the projected hydrological
regimes of Swiss catchments. Water Resour. Res., 50(10), 7541–7562. doi:
10.1002/2014WR015549

⁵⁷⁸ Aquanty Inc. (2015). HGS Reference Manual. Waterloo. Retrieved from
`https://static1.squarespace.com/static/54611cc8e4b0f88a2c1abc57/t/`
`59cea33846c3c4384b8e5de1/1506714438873/hydrosphere_user.pdf`

⁵⁸¹ Barthel, R., & Banzhaf, S. (2016). Groundwater and Surface Water Interaction
at the Regional-scale—A Review with Focus on Regional Integrated Models.
Water Resour. Manag., 30(1), 1–32. doi: 10.1007/s11269-015-1163-z

⁵⁸⁴ Barthold, F. K., Tyralla, C., Schneider, K., Vaché, K. B., Frede, H. G., & Breuer,
L. (2011). How many tracers do we need for end member mixing analy-
sis (EMMA)? A sensitivity analysis. Water Resour. Res., 47(8), 1–14. doi:
10.1029/2011WR010604

⁵⁸⁸ Beria, H., Larsen, J. R., Michelon, A., Ceperley, N. C., & Schaefli, B. (2020). Hy-
droMix v1.0: A new Bayesian mixing framework for attributing uncertain
hydrological sources. Geoscientific Model Development, 13(5), 2433–2450. doi:
10.5194/gmd-13-2433-2020

⁵⁹² Blau, R. V., & Muchenberger, F. (1997). Grundlagen für Schutz und Bewirtschaftung der Grundwasser des Kanto
(Tech. Rep.). Bern: Wasser- und Energiewirtschaftsamt des Kantons Bern,
Geotechnisches Institut AG.

⁵⁹⁵ Blöschl, G., Hall, J., Viglione, A., Perdigão, R. A. P., Parajka, J., Merz, B., . . .

Živković, N. (2019). Changing climate both increases and decreases European river floods. Nature, 573(7772), 108–111. doi: 10.1038/s41586-019-1495-6

Boano, F., Harvey, J. W., Marion, A., Packman, A. I., Revelli, R., Ridolfi, L., & Wörman, A. (2014). Hyporheic flow and transport processes: Mechanisms, models, and biogeochemical implications. Rev. Geophys., 52(4), 603–679. doi: 10.1002/2012RG000417

Bourke, S., Cook, P. G., Shanafield, M., Dogramaci, S., & Clark, J. F. (2014). Characterisation of hyporheic exchange in a losing stream using radon-222. J. Hydrol., 519, 94–105. doi: 10.1016/j.jhydrol.2014.06.057

Brennwald, M. S., Schmidt, M., Oser, J., & Kipfer, R. (2016). A portable and autonomous mass spectrometric system for on-site environmental gas analysis. Environ. Sci. Technol., acs.est.6b03669. doi: 10.1021/acs.est.6b03669

Brewer, M. J., Soulsby, C., & Dunn, S. M. (2002). A Bayesian Model for Compositional Data Analysis. In W. Härdle & B. Rönz (Eds.), Compstat (p. 105-110). Physica-Verlag HD.

Brunner, P., & Simmons, C. T. (2012). HydroGeoSphere: A Fully Integrated, Physically Based Hydrological Model. Ground Water, 50(2), 170–176. doi: 10.1111/j.1745-6584.2011.00882.x

Brunner, P., Therrien, R., Renard, P., Simmons, C. T., & Franssen, H.-J. H. (2017, sep). Advances in understanding river-groundwater interactions. Rev. Geophys., 55(3), 818–854. doi: 10.1002/2017RG000556

Carrera, J., Vázquez-Suñé, E., Castillo, O., & Sánchez-Vila, X. (2004). A methodology to compute mixing ratios with uncertain end-members. Water Resour. Res., 40(12), 1–11. doi: 10.1029/2003WR002263

Chatton, E., Labasque, T., de La Bernardie, J., Guihéneuf, N., Bour, O., & Aquilina, L. (2017). Field continuous measurement of dissolved gases with a cf-mims: Applications to the physics and biogeochemistry of groundwater flow. Environmental science & technology, 51(2), 846–854. doi: 10.1021/acs.est.6b03706

Cochand, M., Christe, P., Ornstein, P., & Hunkeler, D. (2019). Groundwater Storage in High Alpine Catchments and Its Contribution to Streamflow. Water Resources Research, 55(4), 2613–2630. doi: 10.1029/2018WR022989

Cook, P., & Herczeg, A. L. (2000). Environmental Tracers in Subsurface Hydrology

(Vol. 53) (No. 9). Springer Science+Business Media New York. doi: 10.1017/CBO9781107415324.004

Delsman, J. R., Oude Essink, G. H., Beven, K. J., & Stuyfzand, P. J. (2013). Uncertainty estimation of end-member mixing using generalized likelihood uncertainty estimation (GLUE), applied in a lowland catchment. Water Resour. Res., 49(8), 4792–4806. doi: 10.1002/wrcr.20341

DURRIDGE. (2019). Rad7 Electronic Radon Detector–User Manual. Billerica, MA 01821: DURRIDGE Company Inc. Retrieved from https://www.durridge.com/documentation/RAD7Manual.pdf

Fiddes, J., Aalstad, K., & Westermann, S. (2019). Hyper-resolution ensemble-based snow reanalysis in mountain regions using clustering. Hydrology and Earth System Sciences, 23(11), 4717–4736. doi: 10.5194/hess-23-4717-2019

Gardner, W. P., Harrington, G. A., Solomon, D. K., & Cook, P. G. (2011). Using terrigenic ^{4}He to identify and quantify regional groundwater discharge to streams. Water Resour. Res., 47(6), 1–13. doi: 10.1029/2010WR010276

Gleeson, T., Manning, A. H., Popp, A., Zane, M., & Clark, J. F. (2018). The suitability of using dissolved gases to determine groundwater discharge to high gradient streams. J. Hydrol., 557, 561–572. doi: 10.1016/j.jhydrol.2017.12.022

Harrington, G. A., Walker, G. R., Love, A. J., & Narayan, K. A. (1999). A compartmental mixing-cell approach for the quantitative assessment of groundwater dynamics in the Otway Basin, South Australia. Journal of Hydrology, 214(1-4), 49–63. doi: 10.1016/S0022-1694(98)00243-1

Hayashi, M. (2019). Alpine Hydrogeology: The Critical Role of Groundwater in Sourcing the Headwaters of the World. Groundwater. doi: 10.1111/gwat.12965

Heaton, T. H. E., & Vogel, J. C. (1981). "Excess air" in groundwater. J. Hydrol., 50, 201–216. doi: 10.1016/0022-1694(81)90070-6

Herbstritt, B., Gralher, B., & Weiler, M. (2019). Continuous, near-real-time observations of water stable isotope ratios during rainfall and throughfall events. Hydrol. Earth Syst. Sci., 23(7), 3007–3019. doi: 10.5194/hess-23-3007-2019

Hock, R., Rasul, G., Adler, C., Cáceres, B., Gruber, S., Hirabayashi, Y., ... Steltzer, H. I. (2019). Chapter 2: High Mountain Areas (Tech. Rep.). High Mountain Areas. In: IPCC Special Report on the Ocean and Cryosphere in a Chang-

ing Climate [H.-O. Pörtner, D.C. Roberts, V. Masson-Delmotte, P. Zhai, M. Tignor, E. Poloczanska, K. Mintenbeck, A. Alegría, M. Nicolai, A. Okem, J. Petzold, B. Rama, N.M.

Hoehn, E., & Von Gunten, H. R. (1989). Radon in groundwater: A tool to assess infiltration from surface waters to aquifers. Water Resour. Res., 25(8), 1795–1803. doi: 10.1029/WR025i008p01795

Hoehn, E., Von Gunten, H. R., Stauffer, F., & Dracos, T. (1992). Radon-222 as a Groundwater Tracer. A Laboratory Study. Environ. Sci. Technol., 26(4), 734–738. doi: 10.1021/es00028a010

Hoffmann, R., Goderniaux, P., Jamin, P., Chatton, E., de La Bernardie, J., Labasque, T., ... Dassargues, A. (2020). Continuous dissolved gas tracing of fracture-matrix exchanges. Geophysical Research Letters, 47(17), e2020GL088944. doi: 10.1029/2020GL088944

Holman, I. P. (2006). Climate change impacts on groundwater recharge- uncertainty, shortcomings, and the way forward? Hydrogeol. J., 14(5), 637–647. doi: 10.1007/s10040-005-0467-0

Hooper, R. P. (2003). Diagnostic tools for mixing models of stream water chemistry. Water Resour. Res., 39(3), 55–61. doi: 10.1029/2002WR001528

Hooper, R. P., Christophersen, N., & Peters, N. E. (1990). Modelling streamwater chemistry as a mixture of soilwater end-members - An application to the Panola Mountain catchment, Georgia, U.S.A. J. Hydrol., 116(1-4), 321–343. doi: 10.1016/0022-1694(90)90131-G

Huss, M., & Hock, R. (2015). A new model for global glacier change and sea-level rise. Front. Earth Sci., 3, 1–22. doi: 10.3389/feart.2015.00054

Jacoby, W. G. (2000). Loess: a nonparametric, graphical tool for depicting relationships between variables. Elect. Stud., 19(4), 577–613. doi: 10.1016/S0261-3794(99)00028-1

Jasechko, S. (2019). Global Isotope HydrogeologyReview. Reviews of Geophysics, 57(3), 835–965. doi: 10.1029/2018RG000627

Jonas, T., Marty, C., & Magnusson, J. (2009). Estimating the snow water equivalent from snow depth measurements in the Swiss Alps. J. Hydrol., 378(1-2), 161–167. doi: 10.1016/j.jhydrol.2009.09.021

Käser, D., & Hunkeler, D. (2015). Contribution of alluvial groundwater to the out-

flow of mountainous catchments. Water Resour. Res., 51, 9127–9140. doi: 10
.1002/2014WR016259

Krause, S., Boano, F., Cuthbert, M. O., Fleckenstein, J. H., & Lewandowski, J.
(2014). Understanding process dynamics at aquifer-surface water inter-
faces: An introduction to the special section on new modeling approaches
and novel experimental technologies. Water Resour. Res., 50(2), 1847–1855.
doi: 10.1002/2013WR014755

Krishnaswami, S., Graustein, W. C., Turekian, K. K., & Dowd, J. F. (1982).
Radium, thorium and radioactive lead isotopes in groundwaters: Appli-
cation to the in situ determination of adsorptiondesorption rate constants
and retardation factors. Water Resour. Res., 18(6), 1663–1675. doi:
10.1029/WR018i006p01663

Lewandowski, J., Arnon, S., Banks, E., Batelaan, O., Betterle, A., Broecker, T., . . .
others (2019). Is the hyporheic zone relevant beyond the scientific community?
Water, 11(11), 2230. doi: 10.1002/2016WR019516

Mächler, L., Brennwald, M. S., & Kipfer, R. (2012). Membrane inlet mass spectrom-
eter for the quasi-continuous on-site analysis of dissolved gases in groundwater.
Environ. Sci. Technol., 46(15), 8288–8296. doi: 10.1021/es3004409

Magnusson, J., Gustafsson, D., Hüsler, F., & Jonas, T. (2014). Assimila-
tion of point SWE data into a distributed snow cover model comparing
two contrasting methods. Water Resour. Res., 50(10), 7816–7835. doi:
10.1002/2014WR015302

McCallum, J. L., Cook, P. G., Brunner, P., & Berhane, D. (2010). Solute dynamics
during bank storage flows and implications for chemical base flow separation.
Water Resour. Res., 46(7), 1–11. doi: 10.1029/2009WR008539

Michel, A., Brauchli, T., Lehning, M., Schaefli, B., & Huwald, H. (2020). Stream
temperature and discharge evolution in Switzerland over the last 50 years:
annual and seasonal behaviour. Hydrol. Earth Syst. Sci., 24(1), 115–142. doi:
10.5194/hess-24-115-2020

Mutiti, S., & Levy, J. (2010). Using temperature modeling to investigate the tempo-
ral variability of riverbed hydraulic conductivity during storm events. Journal
of Hydrology, 388(3-4), 321–334. doi: 10.1016/j.jhydrol.2010.05.011

Paniconi, C., & Putti, M. (2015). Physically based modeling in catchment hydrol-

ogy at 50: Survey and outlook. Water Resour. Res., 51(9), 7090–7129. doi: 10 .1002/2015WR017780

Partington, D., Brunner, P., Simmons, C., Therrien, R., Werner, A., Dandy, G., & Maier, H. (2011). A hydraulic mixing-cell method to quantify the groundwater component of streamflow within spatially distributed fully integrated surface watergroundwater flow models. Environ. Model. Softw., 26(7), 886–898. doi: 10.1016/j.envsoft.2011.02.007

Partington, D., Therrien, R., Simmons, C. T., & Brunner, P. (2017). Blueprint for a coupled model of sedimentology, hydrology, and hydrogeology in streambeds. Reviews of Geophysics, 55(2), 287–309. doi: 10.1002/2016RG000530

Popp, A. L., Manning, C. C., Brennwald, M. S., & Kipfer, R. (2020). A New in Situ Method for Tracing Denitrification in Riparian Groundwater. Environmental Science & Technology, 54(3), 1562–1572. doi: 10.1021/acs.est.9b05393

Popp, A. L., Scheidegger, A., Moeck, C., Brennwald, M. S., & Kipfer, R. (2019). Integrating Bayesian groundwater mixing modeling with on-site helium analysis to identify unknown water sources. Water Resour. Res., 55(12), 10602–10615. doi: 10.1029/2019WR025677

Rao, B. K., & Hathaway, D. L. (1989). A Three-Dimensional Mixing Cell Solute Transport Model and Its Application. Ground Water, 27(4), 509–516. doi: 10 .1111/j.1745-6584.1989.tb01971.x

Schilling, O. S., Cook, P. G., & Brunner, P. (2019). Beyond Classical Observations in Hydrogeology: The Advantages of Including Exchange Flux, Temperature, Tracer Concentration, Residence Time, and Soil Moisture Observations in Groundwater Model Calibration. Rev. Geophys., 57(1), 146–182. doi: 10.1029/2018RG000619

Schilling, O. S., Cook, P. G., Grierson, P. F., Dogramaci, S., & Simmons, C. T. (2020). Controls on interactions between surface water, groundwater and riverine vegetation along intermittent rivers and ephemeral streams in arid regions. Water Resources Research, e2020WR028429.

Schilling, O. S., Gerber, C., Partington, D. J., Purtschert, R., Brennwald, M. S., Kipfer, R., . . . Brunner, P. (2017). Advancing Physically-Based Flow Simulations of Alluvial Systems Through Atmospheric Noble Gases and the Novel ^{37}Ar Tracer Method. Water Resour. Res., 53(12), 10465–10490. doi:

10.1002/2017WR020754

Schilling, O. S., Parajuli, A., Tremblay Otis, C., Müller, T., Antolinez Quijano, W., Tremblay, Y., ... others   (2021).   Quantifying groundwater recharge dynamics and unsaturated zone processes in snow-dominated catchments via on-site dissolved gas analysis.   Water Resources Research, e2020WR028479.   doi: 10.1029/2020WR028479

Schilling, O. S., Park, Y. J., Therrien, R., & Nagare, R. M. (2019). Integrated Surface and Subsurface Hydrological Modeling with Snowmelt and Pore Water FreezeThaw. Groundwater, 57(1), 63–74. doi: 10.1111/gwat.12841

Somers, L. D., McKenzie, J. M., Mark, B. G., Lagos, P., Ng, G. H. C., Wickert, A. D., ... Silva, Y.   (2019).   Groundwater Buffers Decreasing Glacier Melt in an Andean WatershedBut Not Forever.   Geophysical Research Letters, 46(22), 13016–13026. doi: 10.1029/2019GL084730

Sprenger, M., Stumpp, C., Weiler, M., Aeschbach, W., Allen, S. T., Benettin, P., ... Werner, C.   (2019).   The Demographics of Water: A Review of Water Ages in the Critical Zone.   Reviews of Geophysics, 57(3), 800–834.   doi: 10.1029/2018RG000633

Stock, B. C., Jackson, A. L., Ward, E. J., Parnell, A. C., Phillips, D. L., & Semmens, B. X.   (2018).   Analyzing mixing systems using a new generation of Bayesian tracer mixing models. PeerJ, 2018(6), 1–27. doi: 10.7717/peerj.5096

Tang, Q., Schilling, O. S., Kurtz, W., Brunner, P., Vereecken, H., & Hendricks Franssen, H.   (2018).   Simulating FloodInduced Riverbed Transience Using Unmanned Aerial Vehicles, Physically Based Hydrological Modeling, and the Ensemble Kalman Filter.   Water Resources Research, 54(11), 9342–9363.   doi: 10.1029/2018WR023067

Valder, J. F., Long, A. J., Davis, A. D., & Kenner, S. J.   (2012).   Multivariate statistical approach to estimate mixing proportions for unknown end members.   J. Hydrol., 460-461, 65–76. doi: 10.1016/j.jhydrol.2012.06.037

Vautier, C., Abhervé, R., Labasque, T., Laverman, A. M., Guillou, A., Chatton, E., ... de Dreuzy, J.-R.   (2020, feb).   Mapping gas exchanges in headwater streams with membrane inlet mass spectrometry.   Journal of Hydrology, 581, 124398.   Retrieved from https://linkinghub.elsevier.com/retrieve/pii/ S0022169419311333 doi: 10.1016/j.jhydrol.2019.124398

Von Freyberg, J., Studer, B., & Kirchner, J. W. (2017). A lab in the field: High-frequency analysis of water quality and stable isotopes in stream water and precipitation. Hydrology and Earth System Sciences, 21(3), 1721–1739. doi: 10.5194/hess-21-1721-2017

Würsten, M. (1991). GWB–Hydrogeologische Untersuchungen Aeschau: Schlussbericht (Tech. Rep.). Zurich: Geotechnisches Institut.